Evaluating the Effectiveness of Forest Conservation Policies with Multitemporal Remotely Sensed Imagery: A Case Study From Tiantangzhai Township, Anhui, China

Q Zhang, CR Hakkenberg, and C Song, University of North Carolina at Chapel Hill, Chapel Hill, NC, United States

Introduction

Global Forest Decline and Forest Conservation

Forests play a key role in providing essential goods and services to humankind, such as food and fiber, soil and water conservation, wildlife habitat, and carbon storage (DeFries et al., 2004; Daily, 1997; MEA, 2005). Alongside tremendous global economic and population growth over the last few decades, global forests have been profoundly altered and modified due to the utilization (and overexploitation) of forest resources (Rudel et al., 2005). Many of the detrimental anthropogenic impacts on global forests have taken place in developing countries, directly influencing as many as 400 million people (Allen and Barnes, 1985) to varying degrees. According to the Global Forest Resources Assessment 2010, the total area (TA) of forests worldwide is decreasing at a rate of 13 million hectares per year—a trend expected to continue into the near future (FAO, 2010). In addition to deforestation, forest degradation poses a tremendous threat to the maintenance of ecosystem services (FAO, 2010). In addition, the global consumption of timber from natural forests generates carbon dioxide accounting for 20% of total fossil fuel emissions and is thus a primary culprit in the acceleration of global warming (van der Werf et al., 2009). Awareness of global forest cover loss has accelerated efforts by governments, communities, and international organizations to devise policies to curb the most destructive timber harvesting practices, such as clear-cutting.

Under the umbrella of climate change mitigation, a set of projects known as reducing emissions from deforestation and forest degradation (REDD and later REDD+) have been initiated to foster forest conservation and carbon storage, with a distinct focus on community livelihoods (Caplow et al., 2011; Groom and Palmer, 2012). These conservation programs employ a variety of innovative policy instruments and have been advocated by researchers and policy-makers alike (Pattanayak et al., 2010; Angelsen, 2009). Payment for ecosystem services (PES) is the most prominent policy measure in the REDD+ toolbox. PES requires a voluntary transaction with well-defined services from buyers to providers who secure the service provision (Wunder, 2008). The REDD+ PES scheme is distinct from other approaches due to its high capital investments and its dual goal of forest conservation/rehabilitation and rural livelihoods (Groom and Palmer, 2012). Integral to the successful implementation and expansion of large-scale PES programs is the requisite attention to active monitoring and objective evaluation of their efficacy in ensuring positive

social–ecological outcomes (Ferraro and Pattanayak, 2006). In this regard, the assessment of forest conservation outcomes necessitates monitoring not only the quantity but also the quality of forest cover as relates to explicitly stated conservation goals.

The Application of Remote Sensing to Forest Growth Monitoring

In light of the enormous cost of traditional ground-based assessments of forest cover change, remote sensing has emerged as a key technology for monitoring forest cover dynamics over large areas (Xie et al., 2008). The abundance of remotely sensed imagery and products from multiple data archives makes it increasingly tractable to synoptically observe spatiotemporal patterns and processes of the Earth surface. For example, open access to Landsat imagery has made it possible for researchers to compile current and historical time series of land cover change (Woodcock et al., 2008), while WorldView-2 (WV-2) data, though costly, enable users to obtain detailed satellite imagery at submeter resolution (Lillesand and Kiefer, 1994).

One of the most prominent applications of remote sensing is the observation and quantification of large-scale patterns in forest cover. Remotely sensed data have been utilized to explore the composition and configuration of terrestrial ecosystems of importance to biodiversity conservation (Horning et al., 2010), forest regeneration and successional processes (Song et al., 2015; Wulder, 1998; Fuller, 2006), and forest management (Franklin, 2001). Remotely sensed vegetation indicators created from spectral bands of satellite images, like the normalized difference vegetation index (NDVI), have been widely used in forest mapping efforts (Calera et al., 2001) and for examining the complexity of canopy structure (Gamon et al., 1995; Soudani et al., 2012). The Tasseled Cap transformation, which linearly converts the multiband spectral signal of Landsat satellite data into a reduced set of interpretable measures (e.g., brightness, greenness, and wetness), is another commonly used remotely sensed index of vegetation cover that has proved to be informative in distinguishing young forests from mature and old-growth ones (Fiorella and Ripple, 1993a; Kauth and Thomas, 1976; Cohen et al., 1995). For example, Song et al. (2007) simulated the spectral reflectance of forest succession, using regression analysis to model the successional trajectories of Tasseled Cap pixel values. Their results indicate that brightness and greenness performed better than wetness for tracking forest succession, highlighting the effectiveness of multitemporal Landsat imagery for the monitoring of large-scale successional processes. However, when characterizing the spectral/temporal trajectories of early successional forests, several sources of uncertainty—caused by topography, atmospheric condition, phenology, and sun/view angles—add noise to the NDVI and Tasseled Cap signal, which may hinder the accurate estimation of forest successional stages (Song et al., 2002). In another study, Fiorella and Ripple (1993b) found a high correlation between the age of Douglas-fir stands and the remote sensing-derived structural index (SI), which can be used to distinguish poorly growing forests from well-regenerated ones. Despite numerous studies exploring the spectral features of forest succession and regeneration, there has been a paucity of research specifically focusing on the evaluation of forest policy interventions on large-scale forest growth trends using multitemporal remotely sensed imagery.

China's Forest Policies

In the first few decades after the establishment of the People's Republic of China in 1949, unsustainable timber production and the general overexploitation of forest resources severely compromised the rise of China's economy (Rozelle et al., 1997; Zhang and Song, 2006). By the late 1990s, the impact of a series of natural disasters was exacerbated by a half-century of rampant deforestation and inadequate soil and water conservation policy, eventually leading to the Yangtze River floods in 1998, which were responsible for 1320 deaths and 20 billion dollars in damage (Zong and Chen, 2000). In response to these disasters, the Chinese government adopted a series of new PES forest policies (Liu et al., 2008). Chief among them was the Conversion of Cropland to Forest Program (CCFP), which aims at soil and water conservation as well as poverty relief (Mullan et al., 2010). Meanwhile, the Chinese government enhanced another policy instrument—its nature reserve system—to prevent logging in large swathes of natural forests designated as public welfare forests (PWFs).

The CCFP incentivizes farmers to convert croplands on steep slopes or other ecologically sensitive areas to forests (China-State-Council, 2002). The CCFP was initiated with different payment schemes in two distinct regions based on the opportunity cost of planting crops: 230 RMB $mu^{-1}year^{-1}$ (mu: a traditional area unit used by farmers in China; 1 mu = 1/15 ha) in the Yangtze River Basin and 160 RMB $mu^{-1}year^{-1}$ in the Yellow River Basin. Initial contracts had an 8-year duration, and participating farmers could renew for another 8-year period at lower compensation rates of 125 RMB $mu^{-1}year^{-1}$ and 90 RMB $mu^{-1}year^{-1}$ in the Yangtze River Basin and the Yellow River Basin, respectively. In PWFs, all commercial logging is prohibited, effectively conserving these forests from most forms of human disturbance. In response to potential adverse economic effects of this new policy on landholders, the central government compensated households holding PWF land at a rate of 8.75 RMB $mu^{-1}year^{-1}$. Although commercial logging on these lands is still banned, subsistence uses such as fuelwood and nontimber forest product collection are permitted. These two nationwide forest programs are unprecedented in the scale and scope of their financial support from the central government (Liu et al., 2008).

Since the implementation of CCFP and PWF programs, numerous studies have assessed their effectiveness in achieving their socioeconomic outcomes (Xu et al., 2004; Li et al., 2011; Cao et al., 2010). However, the ecological consequences of these programs have been insufficiently examined as researchers play catch-up—in part due to the time lag inherent in the recovery of ecosystem services for slow-growing forests. Although it is still too early to fully evaluate these forest programs' success in achieving their water and soil conservation goals, tracking early growth and canopy development trends in the PWFs and newly established CCFP forest stands can be of critical importance in gauging their long-term sustainability.

This article examines results of a case study from Tiantangzhai township in Anhui province to evaluate the effectiveness of the PWF and CCFP forest conservation policies. Our objectives are to (1) create classified maps of forest cover in Tiantangzhai township using a time series of remotely sensed imagery from 1992 to 2013, (2) observe the dynamics of natural forest cover before and after program implementation in 2002 and analyze emerging forest landscape patterns, and finally (3) characterize forest growth trends and canopy development in PWF and CCFP forest stands, based on changes in their spectral trajectories in multitemporal remotely sensed imagery. These research objectives are guided by two interrelated questions: (1) In what ways has forest land cover and land use changed in the study area since the implementation of the CCFP in 2002? (2) What growth trends are observable in PWF and CCFP forest stands since the implementation of the two programs? We hypothesize that Tiantangzhai township experienced an expansion in the quantity (areal extent) of natural forest cover as well as an increase in the quality (successional canopy development) of those forests since policy implementation.

Study Area, Data, and Methods

Study Area

The study area encompasses Tiantangzhai township, located in the eastern part of the Dabieshan Mountain in western Anhui province, China (Fig. 1). The abundantly forested township spans an area of 28,914 ha and lies at an elevation ranging from 300 to 1700 m above sea level. With mild weather and annual rainfall averaging 1350 mm, Tiantangzhai's climate is conducive to high vegetative productivity. Despite its relative proximity to large cities, its extreme topography and poorly developed transportation system have made it geographically inaccessible and sparsely populated, with a rural population of only 17,000 (Yang et al., 2009). Tiantangzhai's historical remoteness is partly responsible for the lack of widespread anthropogenic impact on the region's forests and has helped ensure the preservation of the integrity of its natural ecosystem. Despite this, local resource extraction such as timber harvest and animal hunting has partly undermined larger scale environmental protection efforts by the turn of the 21st century.

In 1998, the Tiantangzhai region was established as a national nature reserve, and all natural forests were designated as PWF. The goal of this program was to protect PWFs from human interference, especially timber and wild animal resource extraction. In 2002, the central government implemented the CCFP, with nearly 20% of all households in Tiantangzhai participating in the program within the first year.

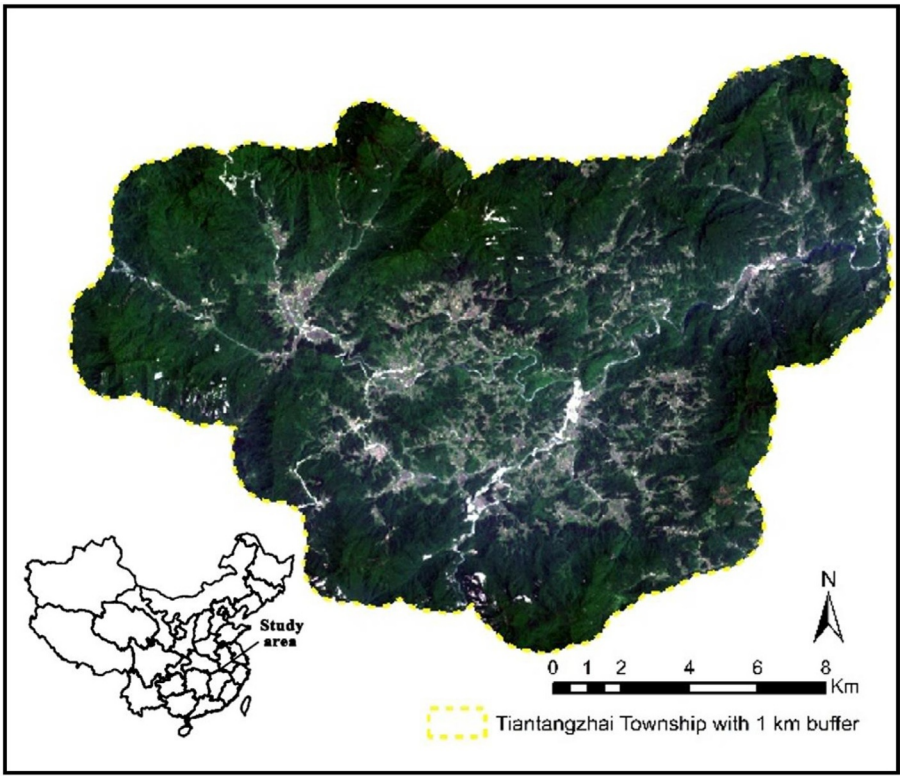

Fig. 1 Study area: Tiantangzhai township in Anhui, China.

Data Acquisition and Preprocessing

Three Landsat images covering the areal extent of the study area were acquired corresponding to the dates Oct. 18, 1992 (Landsat 5 TM), Oct. 6, 2002 (Landsat 7 ETM+), and Oct. 12, 2013 (Landsat 8 OLI). One high spatial resolution WV-2 image from 2013 was also acquired, primarily for reference and analysis of CCFP stands for which Landsat imagery is too coarse (**Table 1**). Prior to the analysis, all Landsat images were atmospherically corrected using simple dark object subtraction (DOS3), converting digital number (DN) values to surface reflectance (Song, 2001). In addition, a set of vegetation indexes were generated from the atmospherically corrected Landsat images and added to the spectral bands (**Table 2**). A digital elevation model at 30 m resolution was obtained from the United States Geological Survey (USGS) for the area and was geographically corrected to align with pixels in the Landsat imagery to generate elevation, slope, and topographic wetness index (TWI) values (Moore et al., 1991; Beven and Kirkby, 1979) (**Table 2**). Ancillary data used in the analysis also include a map provided by the Tiantangzhai forestry station, delineating the extent of each CCFP forest stand within the township.

Classification of Imagery and CCFP Forest Stand Delineation

Inference of forest growth and development trends is based on an analysis of multitemporal land cover maps classified from Landsat imagery. Eight land cover types were defined in the study area for classification: developed area (mainly impervious surfaces), deciduous forests, coniferous forests, mixed forests (including both deciduous and coniferous), water, cropland (paddy and dry cropland), barren land (including exposed rock, soil, and sand), and grassland. Training data for the classification of the 2013 Landsat image were obtained from two data sources: 98 training sites collected using Global Positioning System units in the field during the summer of 2013 and a 2 m resolution WV-2 image from that same year. We randomly selected and reserved 20% of these training sites for accuracy assessment for the classification of the 2013 Landsat reference map.

To create the reference map from the 2013 Landsat image, a random forest (RF) classifier was trained from the WV-2 image. The RF classifier is an ensemble of tree classifiers, where each tree casts an unweighted vote for the prediction of unknown pixels (Breiman, 2001). In this study, each tree was grown with a randomized subset of four features, and 1000 trees were generated to create the ensemble from which the final classification could be inferred based on the majority vote of all trees (Pal, 2005). Predictors used to train the RF model include spectral reflectance, vegetation indexes, and topographic indexes (see **Table 2**). Unlike the 2013 imagery, which was trained with temporally consistent high-resolution reference imagery and field data, training data for the 1992 and 2002 images were not available. To circumvent this shortcoming, training data corresponding to the historical Landsat images (1992 and 2002) were generated algorithmically via the automatic adaptive signature generation (AASG) method (Gray and Song, 2013).

The AASG algorithm is based on the assumption that over a sufficiently large area, the majority of land cover types will not change, and thus, class signatures can be derived independently from stable locations with respect to land cover for each image in a time series (Li et al., 2015; Stow et al., 2014; Kim et al., 2014). Thus, land cover training sites derived from stable locations and labeled according to an existing land cover map are consistent despite radiometric variation between dates due to atmospheric

Table 1 Satellite imagery acquired for the year of 1992, 2002, and 2013

Year	*Date*	*Satellite*	*Sensor*	*Multispectral resolution (m)*	*Panchromatic resolution (m)*
1992	Oct. 18	Landsat 5	TM	30	15
2002	Oct. 6	Landsat 7	ETM+	30	15
2013	Oct. 12	Landsat 8	OLI	30	15
2013	Jul. 13	WorldView-2	-	2	0.5

Landsat imagery corresponds to path/row: 122/38.

Table 2 Description of vegetation and topographic indexes

Index	*Measures*
Vegetation indexes	
Simple ratio (SR) (Hall et al., 1995)	Green vegetation
Normalized difference vegetation index (NDVI) (Purevdorj et al., 1998)	Green vegetation
Structural index (SI) (Fiorella and Ripple, 1993a)	Canopy structure
Normalized difference water index (NDWI) (Gao, 1996)	Vegetation water content in leaves
Enhanced vegetation index (EVI) (Jiang et al., 2008)	Vegetation structure
Topographic indexes	
Elevation (m)	
Slope (degree)	
Topographic wetness index (TWI) (Beven and Kirkby, 1979)	Soil moisture

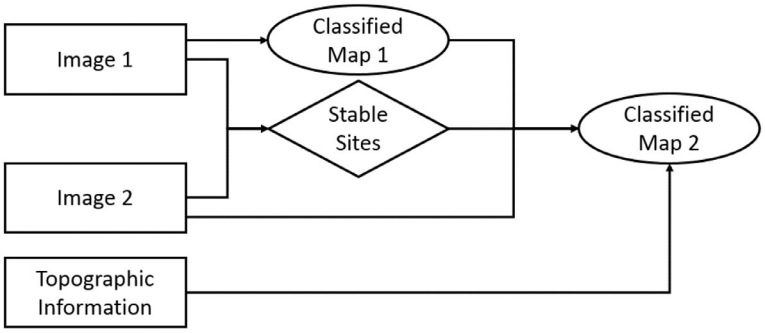

Fig. 2 Workflow for the AASG method (taken from Gray, J. and Song, C. (2013). Consistent classification of image time series with automatic adaptive signature generalization. *Remote Sensing of Environment* **134**, 333–341). The reference image (Image 1) was classified using training data from a WV-2 image and ground points to produce the classification map (Classified Map 1). Training sites for the target image (Image 2) were automatically derived from stable pixels identified by image differencing and then used to generate a classification of the target image (Classified Map 2) based on its automatically derived, adapted spectral signature.

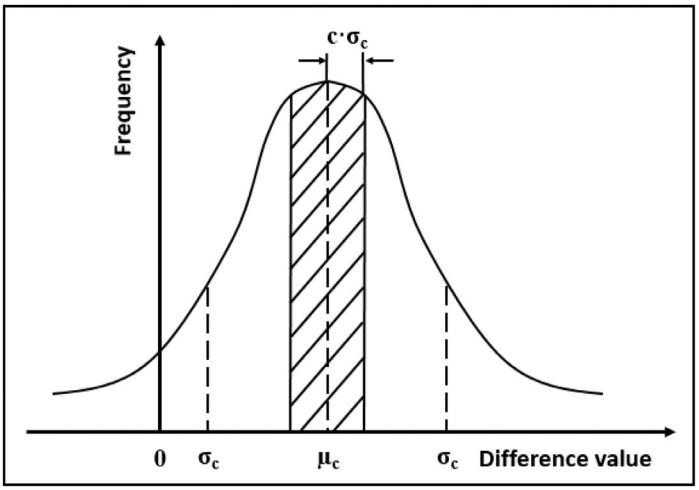

Fig. 3 Selection of the *c* parameter for one class. If the scene extent covers a sufficiently large area and the majority of the pixels are stable, the histogram of single-band differences from the two images assumes a normal distribution. After application of a spatial erode function to ensure pixels emanate from core areas within particular classes, stable pixels are selected that fall within the range of the mean of the histogram (*hatched area*). The symbols μ_c and σ_c denote the mean and standard deviation of the difference values, respectively.

effects, varying irradiance, and other radiometric effects (Fig. 2). Stable sites are selected based on a histogram of the single-band difference of the two images, with stable sites expected to be located around the mean of the image difference histogram and class changes most likely falling within the tails of the distribution (Fig. 3). Stable pixels are identified as those within a certain interval around the histogram mean, defined as $\mu_c \pm c \cdot \sigma_c$, where μ_c and σ_c are the mean and standard deviation of the difference values, respectively, and c is a user-defined constant determining the width of the interval. Due to the potential for image misregistration and edge effects especially along class boundaries in multitemporal imagery, a class-specific erode filter based on a user-defined kernel was employed to ensure that only core pixels were retained among the $\mu_c \pm c \cdot \sigma_c$ potential stable sites. After the determination of stable sites, class labels for stable pixels in the target image can be imputed directly from the corresponding pixels in the reference imagery and used to generate a unique spectral profile for classes in the target image.

Because forests were the dominant land cover class in Tiantangzhai township between 1992 and 2013, an image difference histogram based on NDVI values, rather than the red or near-infrared (NIR) band, was judged appropriate. Furthermore, a class-specific rather than global c parameter was chosen to consider the specific distributions of each class (Dannenberg et al., 2015). As such, the c parameter was determined so that 1000 pixels for each class would be included in the interval ($\mu_c \pm c_c \cdot \sigma_c$) of the histogram. When the total number of pixels was smaller than 1000, all the pixels within the interval were selected.

Due to the challenge inherent in distinguishing CCFP forests from natural forests solely based on spectral information from a single WV-2 image, CCFP forest stands were manually delineated in the WV-2 image. This classification was guided by a map obtained from the Tiantangzhai township forest station with locations of the spatial extent of CCFP forest stands. Technicians from the forest station provided assistance in employing this map to identify CCFP patches in the WV-2 image. In all, 225 CCFP forest stands were delineated and overlaid onto the Landsat and WV-2 images.

Growth Trends of Natural Forests and CCFP Forest Stands

Growth trends in PWF and CCFP forests were inferred from remotely sensed forest development indexes based on changes in the distribution of Tasseled Cap values, a linear matrix transformation of spectral bands in Landsat imagery (Crist, 1985). The Tasseled Cap transformation derives its name from the fact that when transformed pixel values are plotted in a two-dimensional brightness–greenness space (B–G space), the emergent pattern of scattered pixels resembles that of a Tasseled Cap (Crist and Cicone, 1984). The Tasseled Cap transformation has been used widely for monitoring forest growth and development partly because the resulting transformed indexes can be readily interpreted with biophysical meanings, such as brightness, greenness, and wetness (Cohen et al., 1995; Song et al., 2002; Jakubauskas, 1996). This analysis focuses on the first two component axes of the Tasseled Cap—brightness (B) and greenness (G). To allow for cross compatibility between images, image values in B–G space were standardized to *z*-scores.

Pixels in B–G space correctly classified as forest are generally observed to be located above other classes on the vertical axis (G) and form an upper boundary of all points, regarded as the canopy closure line (CCL) (**Figs. 4–6**). To identify the CCL in B–G space, the greenness axis was segmented into vertical intervals starting from the point with the lowest brightness value to that with the highest greenness value. Within each vertical segment, the individual point with the lowest brightness value was selected as a canopy closure point. A linear trend line based on canopy closure points was then fit to identify the slope of the CCL. The intercept of the CCL was determined by shifting the trend line so that it intersects the canopy closure point furthest from the trend line (point *e*). In this way, all residual points equal or fall below the CCL on the greenness axis (**Fig. 4**). The upper and lower extremities of the CCL are determined by the maximum and minimum values of all pixels projected onto the CCL (e.g., points c' and b' in **Fig. 5**). In general, forest pixels track the lower bound of the CCL, while other land cover types are dispersed far away from it (**Fig. 6**).

The temporal trend of pixel values in B–G space is informative for assessing canopy development (Song et al., 2007). For example, when a forest stand has just reached canopy closure, its trees are relatively small and uniform in size. In this case, larger brightness and greenness values, located at the upper end of the CCL, would be expected (Song et al., 2002). As a stand continues to grow and develop, individual crowns get larger, while other stems are shaded out and eventually succumb to density-dependent mortality (Peet and Christensen, 1987). The concomitant emergence of large canopy crowns increases canopy shadows. The large canopy shadows of these more mature forests manifest as lower brightness and greenness pixel values, which are located more toward the lower end of the CCL compared with younger continuous canopy stands (Song et al., 2007).

Three indexes were generated to define a pixel's forest growth status based on its position relative to other pixels in the B–G space: the canopy closure index (CCI), the maturity index (MI), and the synergistic successional index (SSI) (see **Fig. 5** for a visual depiction of key variables). The CCI is estimated based on the perpendicular distance of a forest pixel to the CCL and is calculated as

$$\mathrm{CI} = \frac{d_{\max} - d_i}{d_{\max}} \tag{1}$$

where $d_{\max}$ is the distance from the furthest forest pixel in B–G space from the CCL and d_i is the distance of the ith pixel to the CCL. The smaller the value of d_i, the closer the pixel is to CCL and the more likely it is to correspond to a closed canopy forest pixel.

The MI measures the relative developmental stage of a forest within a given image. It represents the location of a pixel's projection onto the CCL and is calculated as

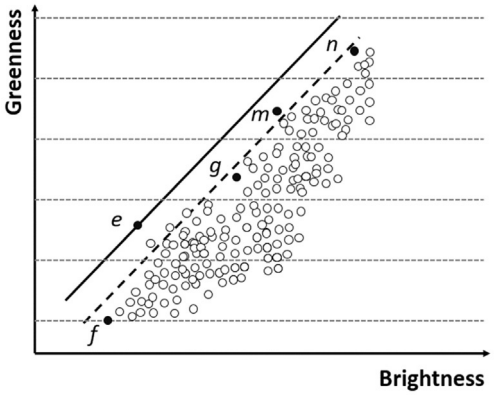

Fig. 4 The canopy closure line (CCL) is defined based on canopy closure points in the brightness–greenness (B–G) space of the Tasseled Cap transformation. Points along the *dashed line* depict the outer edge of the image pixel point cloud. The greenness axis is divided into user-defined vertical segments from *f* (which represents the lowest brightness value) to *n* (which has the highest greenness value). Pixels with the lowest brightness values falling within each vertical greenness segment are called canopy closure points (e.g., *solid points*: *f*, *g*, *e*, *m*, and *n*) and are linearly regressed to define the CCL (*solid line*). Among all the pixel points above the trend line (*dashed line*), *e* has the largest perpendicular distance to the trend line. Therefore, the CCL (*solid line*) is defined by maintaining the slope of the trend line, but modifying its intercept until it intersects *e*. As a result, *e* is the only pixel in the point cloud that lies on the CCL.

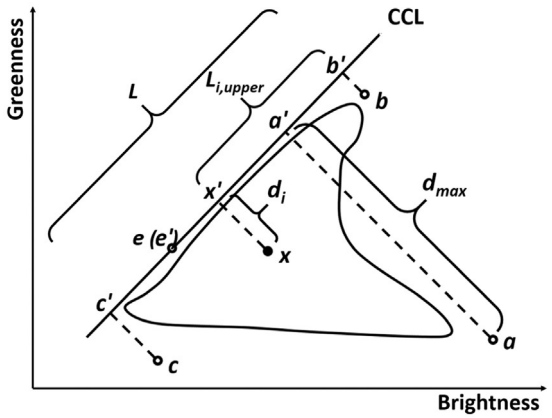

Fig. 5 Key components of the brightness–greenness (B–G) space used for forest development indexes. Point *a* is the pixel with the largest perpendicular distance to the CCL; thus, $d_{max} = |aa'|$. The slope of the CCL is determined by the linear trend line of canopy closure points, while the intercept is set by shifting the trend line to go through $e(e')$ so all the other canopy closure points fall below it. The vertical projection of points *b* and *c* (b' and c') define the upper and lower bounds of the CCL, respectively, with length $L = |c'b'|$. For the *i*th pixel *x*, $d_i = |xx'|$ and $L_{i,\text{upper}} = |x'b'|$. Note that all primes refer to the vertical point projection on the CCL of corresponding points.

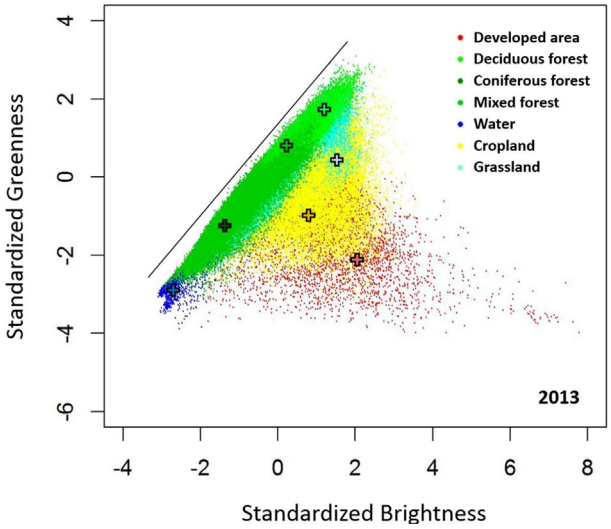

Fig. 6 Scatterplot depicting cover classes in standardized B–G space in the 2013 Landsat 8 OLI image. Mean values of each class are *symbolized as crosses*. The barren land class is not shown due to its small proportion within the overall area.

$$\text{MI} = \frac{L_{i,\text{upper}}}{L} \tag{2}$$

where $L_{i,\text{ upper}}$ is the length of the CCL segment between the upper extremity of the CCL and the location of the *i*th pixel's projection onto the CCL and *L* is the total length of the CCL. In general, larger MI values are indicative of more mature forests.

The SSI was calculated as the product of these two indexes:

$$\text{SSI} = \frac{d_{\max} - d_i}{d_{\max}} \times \frac{L_{i,\text{upper}}}{L} \tag{3}$$

The SSI integrates the status of both canopy closure and maturity information. Generally, larger SSI values correspond to forest pixels closer to the old-growth forest stage, while lower values are indicative of forests in an early successional stage. Index values of CI, MI, and SSI all range from 0 to 1.

Landscape Pattern Analysis

During the past few decades, numerous landscape pattern metrics have been proposed for analyzing the composition and configuration of landscape structure and spatial pattern (Forman and Godron, 1986). A key concept in landscape ecology is the

Table 3 Landscape metrics

Metrics	*Interpretation*
Total area (TA) (Gustafson, 1998)	Total area (m^2) for patch type *i*
Patch density (PD) (O'Neill et al., 1988)	Number of patches of patch type *i* divided by the total landscape area (m^2)
Edge density (ED) (McGarigal and McComb, 1995)	Sum of the lengths (m) of all edge segments of patch type *i*, divided by the total landscape area (m^2)
Mean patch area (MPA) (O'Neill et al., 1988)	Average area (m^2) of patch type *i*
Mean perimeter area ratio (MPAR) (Helzer and Jelinski, 1999)	Mean patch perimeter (m) to area (m^2) ratio for patch type *i*

Fig. 7 Examples of CCFP forest stands at three levels of development according to their SSI values: (A) well developed, (B) moderately developed, and (C) poorly developed. The *green polygons* represent the boundary of the forest stands (reported by Tiantangzhai forestry station) within a fine spatial resolution WV-2 image.

patch, which is defined as a homogenous area distinct from its surrounding in nature or appearance (Kim et al., 2014). Changes in the patchiness of landscape structure triggered by land cover–land use change have a strong influence on fragmentation, biodiversity, and ecosystem function (Wu, 2006; Fahrig, 2003). In this study, forest landscape pattern was analyzed for the postimplementation period of the two forest programs, using the 2013 WV-2 image and delineated CCFP stands. We selected several predefined class-level metrics for the analysis (**Table 3**): TA of all patches, patch density (PD), edge density (ED), mean patch area (MPA), and mean perimeter area ratio (MPAR) (Gustafson, 1998; O'Neill et al., 1988). Calculated landscape metrics were used to compare landscape patterns in 2013 with a simulated landscape where CCFP stands were excluded, to infer the specific effect of the establishment of CCFP stands on landscape structure. This analysis highlights not just the inclusion of new forest areas but the specific development status of each of the CCFP stands based on the previously described forest development indexes.

Manually delineated CCFP forest stands were grouped into three levels based on their SSI values in the most recent period (2002–13). Stands with an SSI difference (i.e., $SSI_{2013} - SSI_{2002}$) above one standard deviation of all CCFP stands were labeled as well-developed stands, stands within one standard deviation of the mean were labeled as moderately developed, while those below one standard deviation were labeled as poorly developed (**Fig. 7**). Well- and moderately developed stands are characterized by high-density canopy, while poorly developed stands have a more open canopy and are composed of a high proportion of exposed ground shrubs and grasses instead of trees. A linear regression model was employed to evaluate the correlation between these derived forest indexes and the vegetation indexes NDVI, SI, and enhanced vegetation index (EVI). In addition, topographic and vegetation indexes were extracted to characterize the relationship between topographic conditions and CCFP forest stands in different successional stages.

Results

Land Cover, Land Use, and Forest Landscape Pattern Change

Classified maps of the three Landsat images in the time series depict land cover patterns in 1992, 2002, and 2013 (**Fig. 8**). Based on a validation dataset consisting of 20% of the training points derived from field data and WV-2 imagery, the overall accuracy for the 2013 reference classification is 93%, with a kappa coefficient of 0.91 (see **Table 4** for a confusion matrix). From 1992 to 2002, the overall area of forest cover in the region was stable, but from 2002 to 2013, it increased by 13.6%. Total cropland area likewise remained stable in the decade before the CCFP, followed by a decline of 9.1% between 2002 and 2013, partially due to the conversion of cropland to forest.

In order to infer the extent to which the establishment of CCFP stands contributed to forest cover and connectivity by 2013, we compared the landscape structural metrics between two groups: all forests excluding CCFP stands versus all forests combined. When withholding CCFP forests, the landscape configuration of the study area in 2013 is significantly different than when all forests are retained (**Fig. 9**). While the inclusion of CCFP forests only has a limited impact on the TA of all forest patches (+0.2%), it leads to a 2.6% decline in PD and a 1.4% decline in ED compared with when they are excluded, indicating net forest aggregation

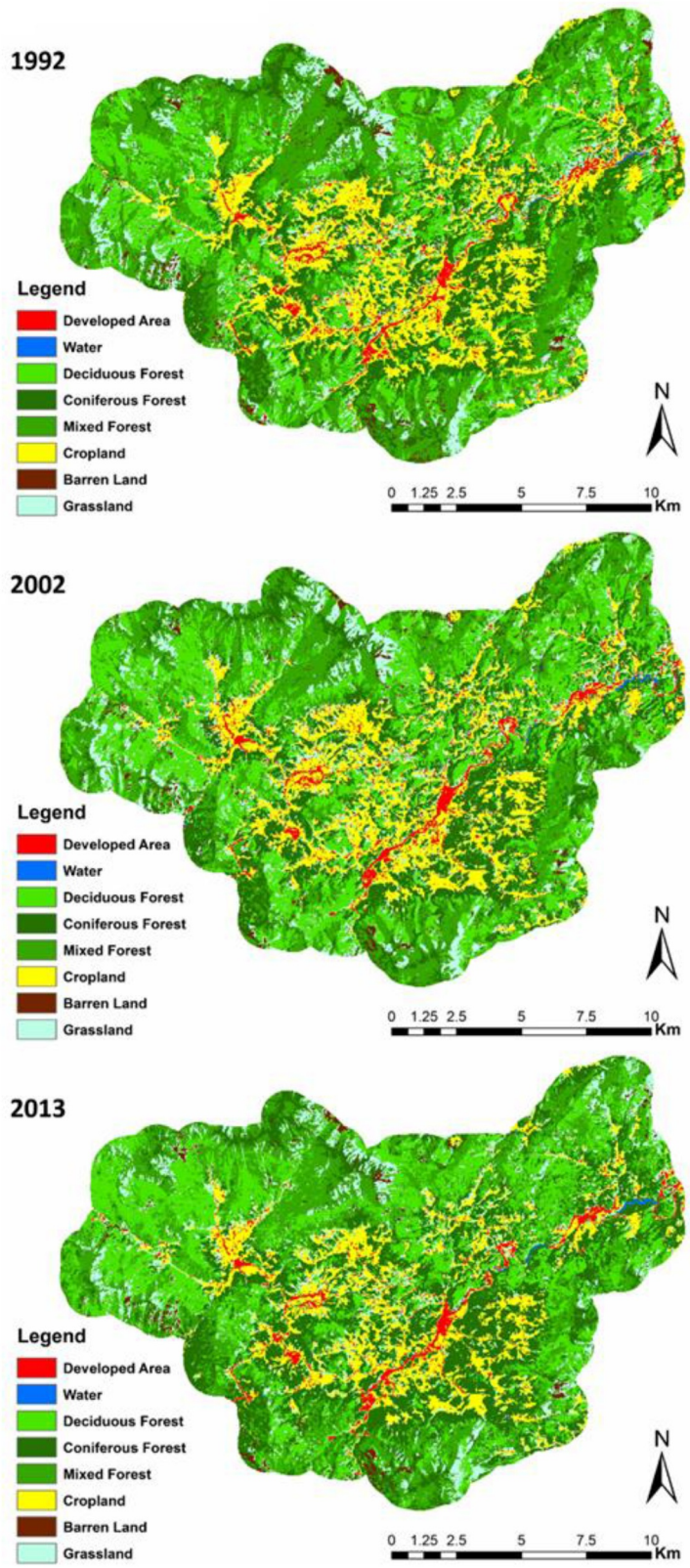

Fig. 8 Land cover maps of the Tiantangzhai township in 1992, 2002, and 2013.

Table 4 Confusion matrix

	Developed area	*Water*	*Deciduous*	*Coniferous*	*Mixed*	*Cropland*	*Barren land*	*Grassland*	*User's accuracy*
Developed	364	0	0	0	0	2	0	0	0.99
Water	0	238	0	0	0	0	0	0	1.00
Deciduous	0	0	67	6	2	0	0	3	0.86
Coniferous	0	0	6	108	9	0	0	0	0.88
Mixed	0	0	5	8	98	0	0	4	0.85
Cropland	6	0	0	0	6	274	0	4	0.94
Barren land	3	0	2	4	2	2	72	2	0.83
Grassland	0	0	0	0	3	9	1	62	0.83
Producer's accuracy	0.98	1.00	0.84	0.86	0.82	0.95	0.99	0.83	0.93

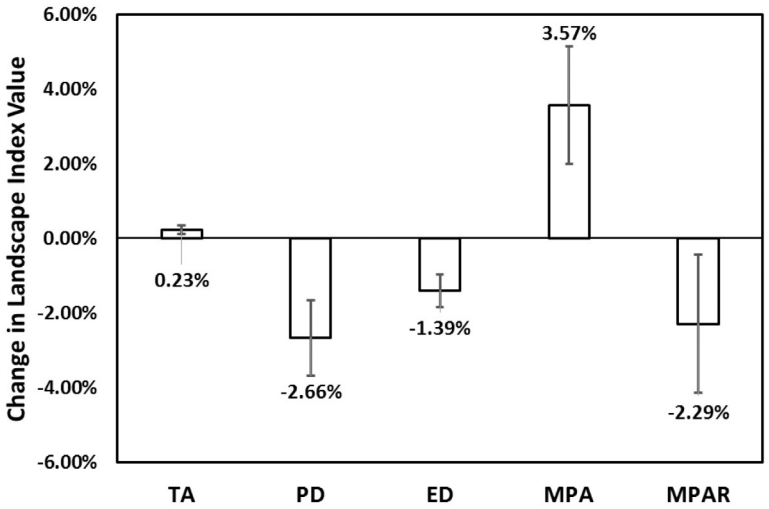

Fig. 9 Percentage change in landscape metric values for forest cover of natural forests when CCFP stands are excluded compared with all forests when CCFP forest stands are retained. *TA*, total area of all patches; *PD*, patch density; *ED*, edge density; *MPA*, mean patch area; *MPAR*, mean perimeter area ratio.

when including the influence of CCFP stands. At the same time, the inclusion of CCFP forest stands increases the MPA (3.6%) and reduces the mean perimeter to area ratio (−2.29%) compared with when they were withheld, indicating that forest patches became slightly less fragmented and isolated with the addition of CCFP stands.

Spectral/Temporal Trajectories in Forest Cover

Spatial–temporal patterns in all land cover classes

The scatterplot of the Tasseled Cap transformation of all pixels from the 2013 Landsat 8 OLI image confirms expectations that pixels corresponding to forest cover are spread linearly along the left side of the Tasseled Cap, with relatively higher greenness values than those from other classes (Fig. 6). Pixels classified as deciduous forest (light green) tend to have higher brightness and greenness values, while coniferous forests (dark green) tend to show lower brightness and greenness values. Mixed forests are located at an intermediate location between the two. While the grassland class has relatively higher brightness values but lower greenness values compared with those of forest pixels, cropland pixels have lower brightness and greenness compared with forest and grassland classes. Heterogeneity in the types of cover (and thus the spectral signature) labeled as developed area results in high variance in the spread of points in the standardized B–G space, though pixels generally tend toward high brightness and low greenness values. Similar scene-wide spectral patterns in the Tasseled Cap transformations are observed in the 1992 Landsat 5 TM image and the 2002 Landsat 7 ETM+ image (not shown).

Temporal trajectories of the mean brightness and greenness values of semantically stable forest pixels indicate that the mixed forest class had the most stable spectral signature through the two decades (Fig. 10). The temporal trajectory of deciduous forests is similar to that of the mixed forests in that both can be characterized by increasing brightness and greenness values, though the two are distinct from that of coniferous forests, where a net decrease in brightness and greenness values was observed. Despite temporal changes in the spectra of stable classes, the general trajectory of mean pixel values supports the observation of a nonlinear spectral trajectory of pixels in B–G space.

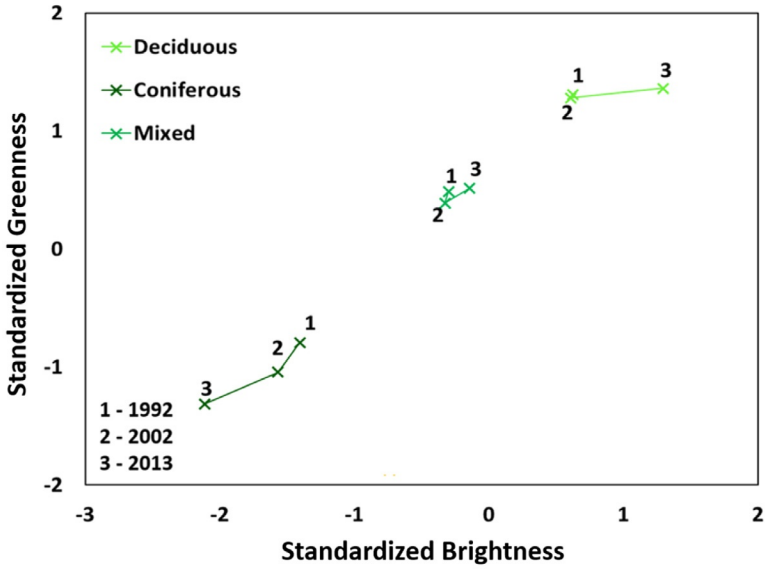

Fig. 10 Temporal trajectories of semantically stable classes in B–G space.

Spectral/temporal trajectories of remotely sensed forest development indexes

In general, change vectors for CCI and SSI values show a trend of net canopy aggradation for all forests during the 2002–13 period (Fig. 11). Temporal trends in CCI values exhibit a decline from 1992 to 2002, followed by a rapid increase coinciding with the advent of the CCFP. MI values, on the other hand, exhibit a flat trajectory from 1992 to 2013. The product of these two indexes, the SSI, follows an intermediate trajectory between the CCI and MI trends that is marked by a distinct increase after 2002. Forest pixels in the 2013 image exhibit higher SSI values than those from images of 1992 and 2002, especially toward the lower left corner of the pixel point cloud, which is composed primarily of coniferous cover pixels (Fig. 12). As brightness and greenness values increase, SSI values decrease as points approach the upper end of the CCL, where pixels corresponding to recently closed canopy stands are located. Pixels in the 1992 and 2002 images are more dispersed and extend farther from the CCL compared with those in the 2013 image, resulting in forest pixels cumulatively possessing higher SSI values in 2013. Scatterplots of SSI values in the 2013 Landsat OLI image show that deciduous forest, which includes CCFP forests, tend to have relatively low SSI values, while coniferous forest have more pixels with higher SSI values than the deciduous and mixed categories (Fig. 13).

Growth Trends in CCFP Forest Stands Based on Remotely Sensed Forest Development Indexes

Temporal trajectories of CCFP forest stands

In total, 225 CCFP forest stands approved by the Tiantangzhai township forest station were manually delineated in the WV-2 image. From 1992 to 2002, the temporal trajectory in standardized B–G space of the mean pixel values of each of the CCFP forest sites exhibited a distinct trend of increasing greenness and stable brightness values (Fig. 14). After 2002 and the implementation of the CCFP, the trajectory of CCFP pixels in B–G space changes course, becoming slightly less green and substantially less bright as CCFP stands were established.

After 2002, the conversion from croplands to forests had a strong influence on CCI values for all CCFP stands. Temporal changes in the remotely sensed forest development indexes show increases in CCI and SSI values and a slight decrease for MI values (Fig. 15). Scatterplots representing the mean of each CCFP forest stand in B–G space in 2002 and 2013 exhibit a similar pattern to those observed for temporal changes in natural forests (Fig. 12), including less dispersion, higher SSI values, and a tighter fit to the CCL in 2013 compared with 2002 (Fig. 16).

Comparison of vegetation indexes for CCFP forest stands

The SI, a ratio of TM or ETM+ bands 4 and 5, can be used as an indicator of canopy structure (Fiorella and Ripple, 1993a). The correlation between CCI, MI, and SSI and SI is generally positive, though the magnitude of correlation varies greatly (Fig. 17). SI was found to have a significant, positive relationship with CCI ($p < 0.05$), but was nonsignificant when regressed against MI ($p = 0.87$). The SI saturates as the SSI increases to 0.3—a result of the negative relationship between SI and MI. When partitioned by the increase of SSI (see section "Landscape Pattern Analysis"), 84% of the CCFP forest stands that were categorized as either well- or moderately developed all exhibited an increase in NDVI, NDWI, EVI, and SI values (Fig. 18). Well- and moderately developed CCFP forests are mainly located in areas of lower elevation (around 610 m) compared with poorly developed stands, which tend to be situated on shallower slopes (Fig. 19).

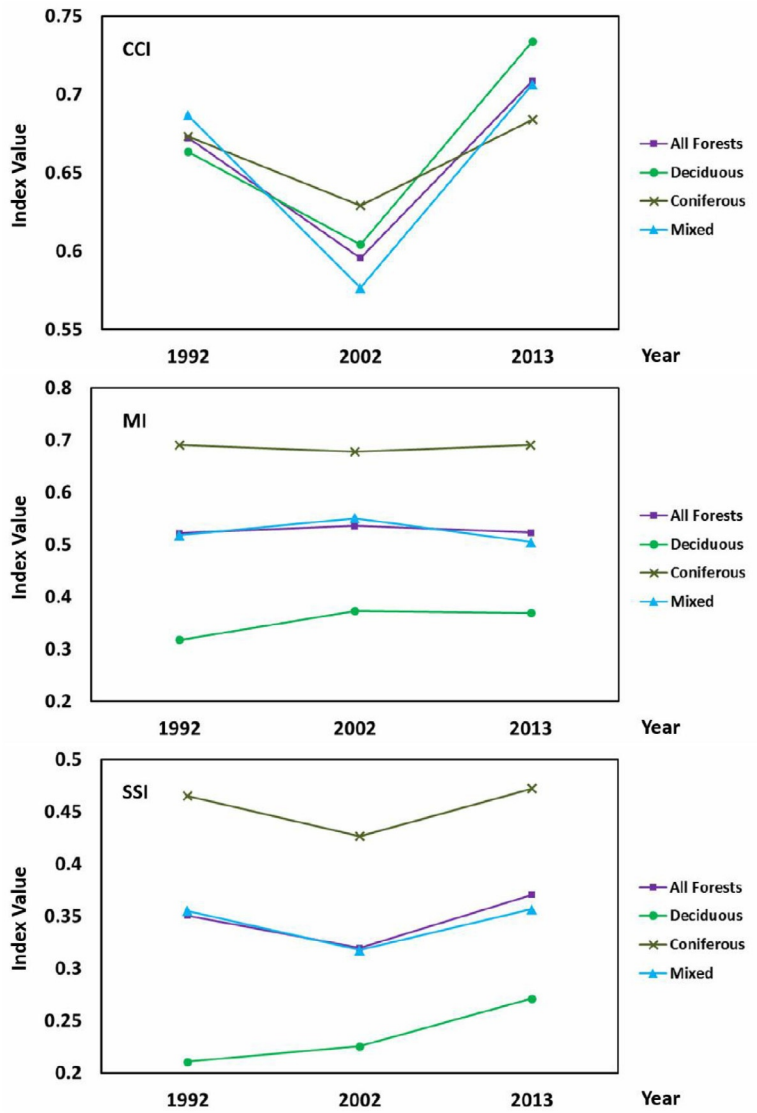

Fig. 11 Temporal change in canopy closure index (CCI), maturity index (MI), and synergistic successional index (SSI) values for deciduous forests, coniferous forests, mixed forests, and all forests.

Discussion

Land Cover Classification and Change Detection

Land parcels in the mountainous region are generally less productive for agriculture at higher elevations. Thus, farmers gradually shifted from farming to other nonfarming activities in these parcels, triggering land abandonment biased toward higher elevations in the late 1990s (De Brauw et al., 2002; Tao et al., 2003). After the implementation of the CCFP, abandoned lands located in ecologically sensitive areas and those on steep, higher elevation slopes were mostly likely to qualify for enrollment in the CCFP. Thus, the increase in the grassland class seen in this analysis before 2002 may be attributed to patterns of cropland abandonment followed by an increase in forest cover after they were converted to forest during the postimplementation period of 2002–13. Much of this enlargement in forest area consists of newly planted deciduous forests as participating households choose to plant ecological trees (e.g., maple) or economic trees (e.g., pecan or walnut) following the CCFP incentive scheme (Uchida et al., 2005). These findings confirm our hypothesis that after the implementation of the CCFP and PWF programs, total forest area increased significantly (14%) in the study area.

Landscape structural analysis revealed that CCFP forests contributed only slightly to the total increase of forest cover by 2013. This is partly due to the modest extent of the 225 stands in comparison with the total study area, as well as the fact that some CCFP stands may not have benefited from proper management by farmers, hindering the aggregation of forest patches throughout the landscape. Though the landscape analysis indicates only slight changes to landscape structure due to the inclusion of CCFP stands,

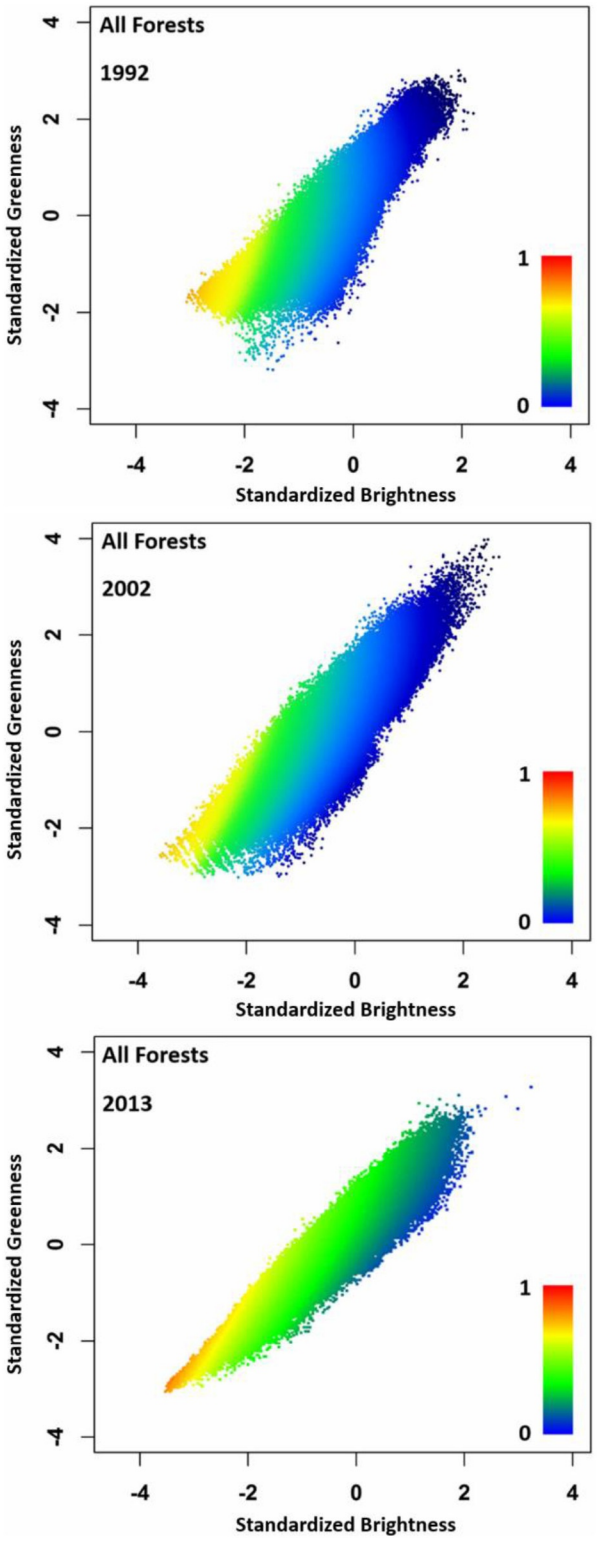

Fig. 12 Scatterplot of SSI pixel values for all forests in 1992, 2002, and 2013 in standardized B–G space.

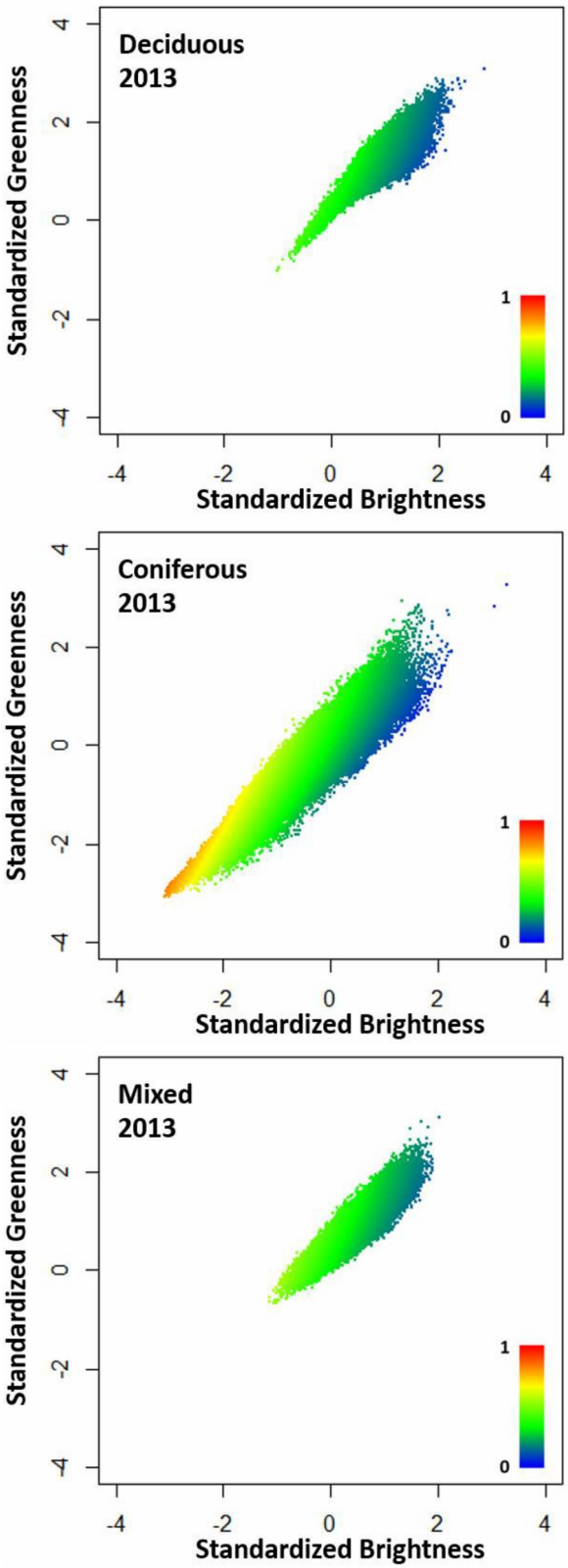

Fig. 13 Scatterplot of SSI values in the 2013 Landsat OLI image split by forest type.

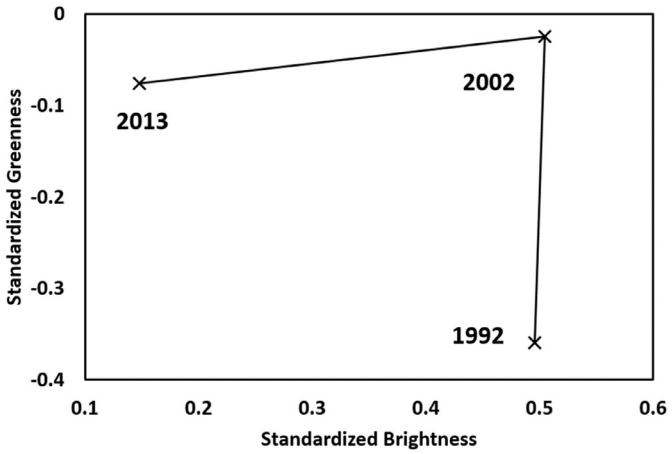

Fig. 14 Temporal trajectory of mean brightness and greenness pixel values of mean values for all CCFP forest stands.

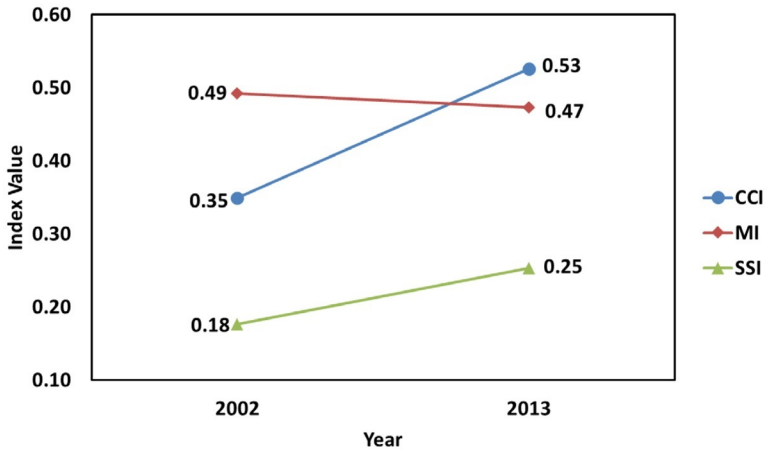

Fig. 15 Temporal change of mean CCI, MI, and SSI pixel values for all CCFP forest stands. Because CCFP forest stands were cropland before the implementation of the CCFP, forest indexes are not applicable before 2002.

results nonetheless show that the forest landscape became less fragmented, and patches became less isolated. This trend was observed for all forests combined, as well as for each individual forest category (deciduous, coniferous, and mixed).

Temporal Trajectories and Growth Trend of Natural Forests and CCFP Stands

The Tasseled Cap transformation is a data reduction method that produces interpretable measures of spectral features in Landsat imagery that perform well for image classification (Fiorella and Ripple, 1993b; Dymond et al., 2002). For the cropland class, reflectance of the bright soil background contributes to higher brightness values, which are only slightly moderated by grass reflectance. In closed canopy forest classes, the spectral signature emanates mainly from the upper canopy rather than the soil background and thus exhibits higher greenness values. Along the CCL, both greenness and brightness values for forest pixels decrease with succession because of mutual shading caused by gap-crown pattern formation. We found that brightness and greenness values for coniferous forests decreased during 2002–13, suggesting mature (mainly coniferous) forests continue to grow after canopy closure. However, both brightness and greenness values for mixed and deciduous forests increased after the CCFP implementation, a result of the emergence of deciduous forests at the establishment stage, where bright soil background is still a factor in pixel-wise reflectance characteristics. For cropland that was stable between dates (i.e., that was neither abandoned nor converted to CCFP stands), observed changes in reflectance may be the result of land use change, such as the conversion of paddy land to dryland, or due to the planting of alternative crops with different spectral–phenological signals (Wang and Maclaren, 2012).

In addition to tracking temporal changes in natural forest area, the CCI, MI, and SSI forest development indexes provide information on how forest canopies are developing at the stand scale. The scene-wide mean CCI experienced its greatest increase after 2002 compared with the decade before the implementation of the CCFP and PWF programs, indicating a general landscape-wide trend toward canopy closure in established forests. The observation of lower MI values for deciduous forests compared with coniferous forests suggests that deciduous forests (including CCFP forest stands) tend to be at an earlier successional stage and were still establishing after conversion from grassland and cropland. Though the increase in SSI for all forests after 2002 is indicative of

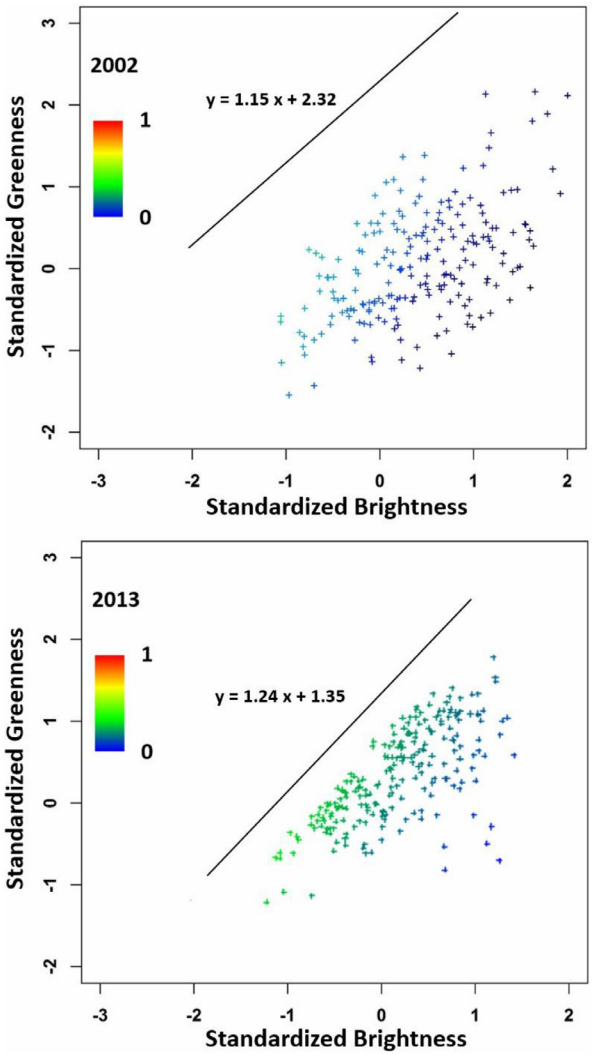

Fig. 16 Scatterplot of mean SSI pixel values for each CCFP forest stand in 2002 and 2013; CCL—*solid line*.

overall successional development for natural forests in the study area, its increase was only slight—due partly to the short time frame of this 11-year analysis. Temporal patterns of mean CCI, MI, and SSI values for CCFP forest stands are similar to those observed in natural forests. The increase of SSI and CCI indicates increased density in CCFP canopies, while the stable MI trend reflects the fact that CCFP forests are still in an establishment stage and will need several decades before reaching maturity. Since priority in CCFP enrollment is given to land parcels in ecologically sensitive areas such as areas with steep slope and thus high risk of soil erosion (Liu et al., 1994), elevation and slope of the CCFP parcels likewise play an important role in forest management by participating households. Based on their SSI values, well-developed CCFP forest stands are more likely to be located in areas of lower elevation and moderate slope. Such topographic conditions are associated with the accessibility of forest stands to farmers, as residents tend to be settled near the township center at lower elevations. As 84% of CCFP forest stands fall into the either well-developed or moderately developed level, overall results confirm a positive growth trend upon the implementation of the CCFP. Looking forward, the success of these early successional CCFP will hinge upon management decisions in the stand establishment stage because only by ensuring the early survival of CCFP forests can participating households receive compensation from the central government (Xu et al., 2010). Our analysis corroborates results from other studies that show that CCFP stands in proximity to these participating households have tended to have received better management—essential to the young forests at the early growing stage (Bennett et al., 2014).

Conclusions

The CCFP is the largest reforestation program in China and among the largest worldwide (Bennett, 2008). According to the Chinese government, the main objective of these new forest policies is for ecosystem service provision, especially soil and water

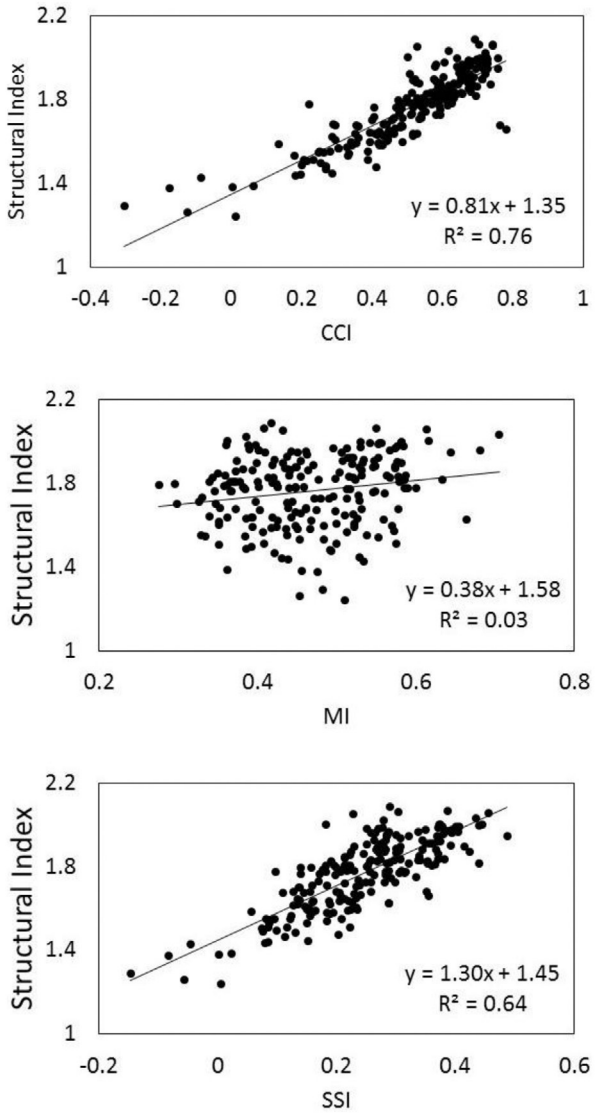

Fig. 17 Linear regression of the structural index (reflectance ratio of TM or ETM+ band 4/band 5) compared with CCI, MI, and SSI values. *Points* represent the mean value of each CCFP forest stand in 2013.

conservation (Liu et al., 2008). Based on official statistics, the Chinese government appears to have accomplished these goals based solely on the increase in total forest area (SFA, 2013). However, reported statistics are not convincing without an accurate accounting of actual landscape forest development. In this study, we employ multitemporal remote sensing analysis to infer the net effect of the CCFP and the PWF forest policies in Tiantangzhai township, Anhui, China. Our results indicate that between 2002 and 2013, substantial land cover changes took place following the implementation of these two programs compared with the decade before. Overall, natural forests increased by 14% from 2002 to 2013, while the area of cropland declined by 9%. This increase in total forest cover likewise resulted in a decline in landscape-wide fragmentation as natural forests received protection and CCFP forest stands were established. CCFP forest stands located in proximity to managing households and occurring in favorable topographic positions experienced accelerated canopy structural development.

In addition to findings concerning the change in the quantity of forest cover extent based on Landsat time series change detection analysis over the entire 20-year period and landscape structural analysis comparing the effect with and without the inclusion of CCFP forests by 2013, we establish three new remotely sensed forest development indexes to assess the quality of those new forests. Specifically, we developed the CCI, the MI, and the SSI to quantify remotely sensed forest canopy development characteristics based on pixel proximity to the CCL in the B–G space of the Tasseled Cap transformation. Results indicate that temporal trends in CI and SSI values over the entire study area exhibit a decline from 1992 to 2002, followed by an increase with the advent of the CCFP and PWF. These findings indicate net forest canopy development in the study area characterized by an increase in canopy density in younger forests as well as increasing canopy complexity in mature forests. Taken together, these results

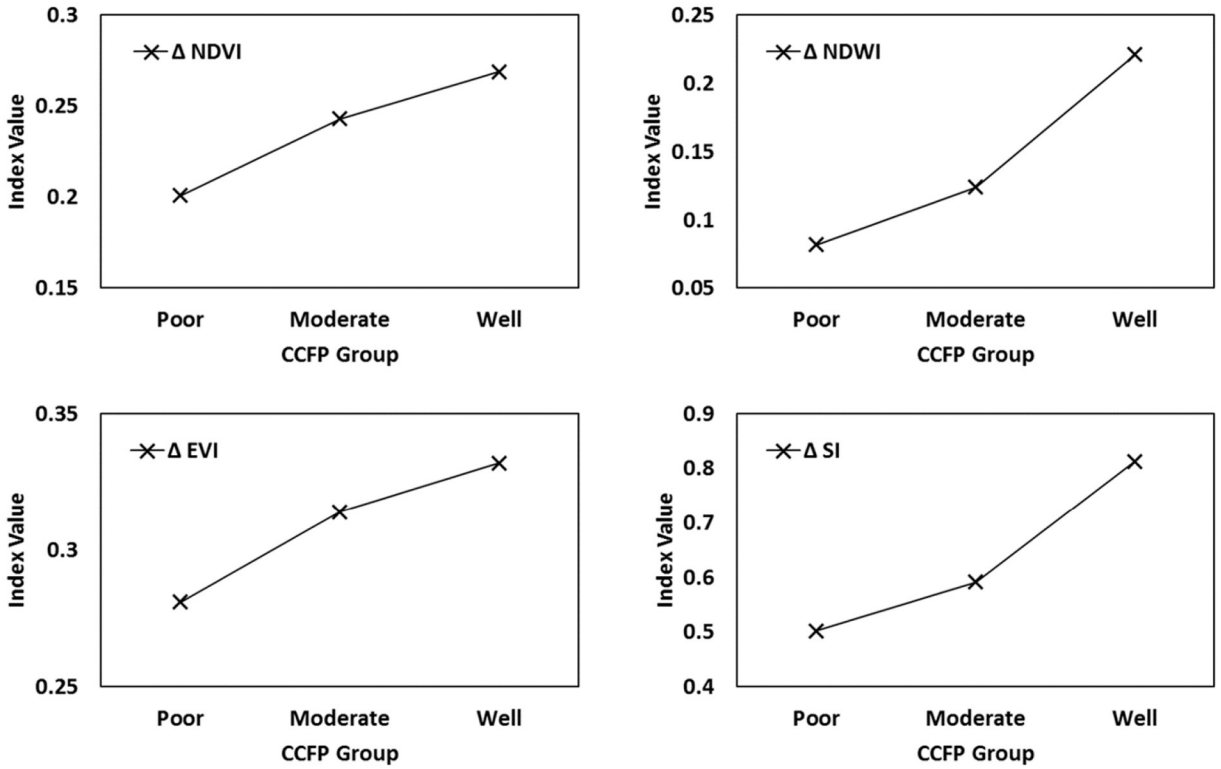

Fig. 18 The differences (Δ) in mean values of NDVI, NDWI, EVI, and SI of CCFP forest stands between 2002 and 2013, grouped by the level of CCFP forest development.

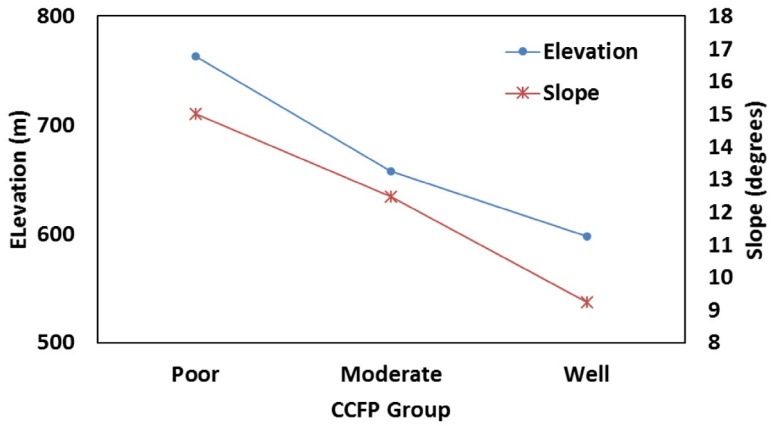

Fig. 19 Proportional distributions of elevation and slope for poorly, moderately, and well-developed CCFP forest stands.

demonstrate the utility of the CI, MI, and SSI forest development indexes for tracking landscape-scale successional processes and confirm our hypothesis that the study area exhibited signs of increasing quantity (areal extent) and quality (canopy development) of forest cover following the implementation of the CCFP and PWF forest policies.

Acknowledgment

This research was supported by the National Science Foundation (Grant No. DEB-1313756).

References

Allen JC and Barnes DF (1985) The causes of deforestation in developing countries. *Annals of the Association of American Geographers* 75(2): 163–184.

Angelsen A (2009) *Realising REDD+: National strategy and policy options*. Bogor: CIFOR.

Bennett MT (2008) China's sloping land conversion program: institutional innovation or business as usual? *Ecological Economics* 65(4): 699–711.

Bennett M, Xie C, Hogarth N, Peng D, and Putzel L (2014) China's conversion of cropland to forest program for household delivery of ecosystem services: How important is a local implementation regime to survival rate outcomes? *Forests* 5(9): 2345–2376.

Beven KJ and Kirkby MJ (1979) A physically based, variable contributing area model of basin hydrology. *Hydrological Sciences Bulletin* 24(1): 43–69.

Breiman L (2001) Random forests. *Machine Learning* 45(1): 5–32.

Calera A, Martínez C, and Meliá J (2001) A procedure for obtaining green plant cover: Relation to NDVI in a case study for barley. *International Journal of Remote Sensing* 22(17): 3357–3362.

Cao S, Wang X, Song Y, Chen L, and Feng Q (2010) Impacts of the natural forest conservation program on the livelihoods of residents of northwestern China: Perceptions of residents affected by the program. *Ecological Economics* 69(7): 1454–1462.

Caplow S, Jagger P, Lawlor K, and Sills E (2011) Evaluating land use and livelihood impacts of early forest carbon projects: Lessons for learning about REDD+. *Environmental Science and Policy* 14(2): 152–167.

China-State-Council (2002) *Notice regarding the improvement of the conversion of cropland to forests policy*. Beijing: State Council of the PRC.

Cohen WB, Spies TA, and Fiorella M (1995) Estimating the age and structure of forests in a multi-ownership landscape of Western Oregon, U.S.A. *International Journal of Remote Sensing* 16(4): 721–746.

Crist EP (1985) A TM tasseled cap equivalent transformation for reflectance factor data. *Remote Sensing of Environment* 17(3): 301–306.

Crist EP and Cicone RC (1984) A physically-based transformation of thematic mapper data: The TM tasseled cap. *IEEE Transactions on Geoscience and Remote Sensing* GE-22(3): 256–263.

Daily GC (1997) *Nature's services: Societal dependence on natural ecosystems*. Ecology, Washington, DC: Island Press p. 392.

Dannenberg MP, Hakkenberg CR, and Song C (2016) Consistent classification of Landsat time series with an improved automatic adaptive signature generalization algorithm. *Remote Sensing*. In Press.

De Brauw A, Huang J, Rozelle S, Zhang L, and Zhang Y (2002) The evolution of China's rural labor markets during the reforms. *Journal of Comparative Economics* 30: 329–353.

DeFries RS, Foley JA, and Asner GP (2004) Land-use choices: Balancing human needs and ecosystem function. *Frontiers in Ecology and the Environment* 2(5): 249–257.

Dymond CC, Mladenoff DJ, and Radeloff VC (2002) Phenological differences in tasseled cap indices improve deciduous forest classification. *Remote Sensing of Environment* 80(3): 460–472.

Fahrig L (2003) Effects of habitat fragmentation on biodiversity. *Annual Review of Ecology, Evolution, and Systematics* 34(1): 487–515.

FAO (2010) *Global forest resources assessment 2010*. FAO forestry paper 163.

Ferraro PJ and Pattanayak SK (2006) Money for nothing? A call for empirical evaluation of biodiversity conservation investments. *PLoS Biology* 4(4): 482–488.

Fiorella M and Ripple W (1993a) Determining successional stage of temperate coniferous forests with Landsat satellite data. *Photogrammetric Engineering and Remote Sensing* 59(2): 239–246.

Fiorella M and Ripple WJ (1993b) Analysis of conifer forest regeneration using Landsat thematic mapper data. *Photogrammetric Engineering & Remote Sensing* 59(9): 1383–1388.

Forman RTT and Godron M (1986) *Landscape ecology*. New York: John Wiley & Sons.

Franklin SE (2001) *Remote sensing for sustainable forest management*. Boca Raton, FL: CRC Press.

Fuller DO (2006) Tropical forest monitoring and remote sensing: A new era of transparency in forest governance? *Singapore Journal of Tropical Geography* 27(1): 15–29.

Gamon JA, Field CB, Goulden ML, Griffin KL, Hartley AE, Joel G, Penuelas J, and Valentini R (1995) Relationships between NDVI, canopy structure, and photosynthesis in three Californian vegetation types. *Ecological Applications* 5(1): 28–41.

Gao BC (1996) NDWI—A normalized difference water index for remote sensing of vegetation liquid water from space. *Remote Sensing of Environment* 58(3): 257–266.

Gray J and Song C (2013) Consistent classification of image time series with automatic adaptive signature generalization. *Remote Sensing of Environment* 134: 333–341.

Groom B and Palmer C (2012) REDD+ and rural livelihoods. *Biological Conservation* 154: 42–52.

Gustafson EJ (1998) Quantifying landscape spatial pattern: What is the state of the art? *Ecosystems* 1(2): 143–156.

Hall FG, Townshend JR, and Engman ET (1995) Status of remote sensing algorithms for estimation of land surface state parameters. *Remote Sensing of Environment* 51(1): 138–156.

Helzer CJ and Jelinski DE (1999) The relative importance of patch area and perimeter-area ratio to grassland breeding birds. *Ecological Applications* 9(4): 1448–1458.

Horning N, Robinson JA, Sterling EJ, Turner W, and Spector S (2010) *Remote sensing for ecology and conservation: A handbook of techniques*. Oxford: Oxford University Press.

Jakubauskas ME (1996) Thematic mapper characterization of lodgepole pine seral stages in Yellowstone National Park, USA. *Remote Sensing Environment* 56(2): 118–132.

Jiang Z, Huete AR, Didan K, and Miura T (2008) Development of a two-band enhanced vegetation index without a blue band. *Remote Sensing of Environment* 112(10): 3833–3845.

Kauth RJ and Thomas GS (1976) The tasselled cap—A graphic description of the spectral-temporal development of agricultural crops as seen by Landsat. In: *Proceedings of the Symposium on Machine Processing of Remotely Sensed Data, West Lafayette, Indiana, U.S.A, 29 June–1 July 1976*, pp. 41–51.

Kim DH, Sexton JO, Noojipady P, Huang C, Anand A, Channan S, Feng M, and Townshend JR (2014) Global, Landsat-based forest-cover change from 1990 to 2000. *Remote Sensing of Environment* 155: 178–193.

Li J, Feldman MW, Li S, and Daily GC (2011) Rural household income and inequality under the sloping land conversion program in western China. *Proceedings of the National Academy of Sciences* 108(19): 7721–7726.

Li X, Gong P, and Liang L (2015) A 30-year, (1984–2013) record of annual urban dynamics of Beijing city derived from Landsat data. *Remote Sensing of Environment* 166: 78–90.

Lillesand TM and Kiefer RW (1994) *Remote sensing and image interpretation*, 3rd edn. New York, NY: John Wiley Sons, Inc. pp. 524–647.

Liu BY, Nearing MA, and Risse LM (1994) Slope gradient effects on soil loss for steep slopes. *Transactions of the American Society of Agricultural Engineers* 37: 1835–1840.

Liu J, Li S, Ouyang Z, Tam C, and Chen X (2008) Ecological and socioeconomic effects of China's policies for ecosystem services. *Proceedings of the National Academy of Sciences of the United States of America* 105(28): 9477–9482.

McGarigal K and McComb WC (1995) Relationships between landscape structure and breeding birds in the Oregon coast range. *Ecological Monographs* 65(3): 235–260.

MEA (2005) Ecosystems and human well-being. Health synthesis. *Ecosystems* 5(281): 1–100.

Moore ID, Grayson RB, and Ladson AR (1991) Digital terrain modeling: A review of hydrological geomorphological and biological applications. *Hydrological Processes* 5(1): 3–30.

Mullan K, Kontoleon A, Swanson TM, and Zhang S (2010) Evaluation of the impact of the natural forest protection program on rural household livelihoods. *Environmental Management* 45(3): 513–525.

O'Neill RV, Krummel JR, Gardner RH, Sugihara G, Jackson B, Deangelis DL, Milne BT, Turner MG, Zygmunt B, Christensen SW, et al. (1988) Indices of landscape pattern. *Landscape Ecology* 1(3): 153–162.

Pal M (2005) Random forest classifier for remote sensing classification. *International Journal of Remote Sensing* 26(1): 217–222.

Pattanayak SK, Wunder S, and Ferraro PJ (2010) Show me the money: Do payments supply environmental services in developing countries? *Review of Environmental Economics and Policy* 4(2): 254–274.

Peet RK and Christensen NL (1987) Competition and tree death. *Bioscience* 37(8): 586–595.

Purevdorj T, Tateishi R, Ishiyama T, and Honda Y (1998) Relationships between percent vegetation cover and vegetation indices. *International Journal of Remote Sensing* 19(18): 3519–3535.

Rozelle S, Huang J, and Zhang L (1997) Poverty, population and environmental degradation in China. *Food Policy* 22(3): 229–251.
Rudel TK, Coomes OT, Moran E, Achard F, Angelsen A, Xu J, and Lambin E (2005) Forest transitions: Towards a global understanding of land use change. *Global Environmental Change* 15(1): 23–31.
SFA (2013) *Forestry development annual report*. Beijing: China Forestry Publishing Press.
Song C (2001) Classification and change detection using Landsat TM data when and how to correct atmospheric effects? *Remote Sensing of Environment* 75(2): 230–244.
Song C, Woodcock CE, and Li X (2002) The spectral temporal manifestation of forest succession in optical imagery. *Remote Sensing of Environment* 82: 285–302.
Song C, Schroeder TA, and Cohen WB (2007) Predicting temperate conifer forest successional stage distributions with multitemporal Landsat thematic mapper imagery. *Remote Sensing of Environment* 106(2): 228–237.
Song C, Chen JM, Hwang T, Gonsamo A, Croft H, Zhang Q, Dannenberg M, Zhang Y, Hakkenberg C, Li J, et al. (2015) Ecological characterization of vegetation using multisensor remote sensing in the solar reflective spectrum. In: *Land resources monitoring, modeling, and mapping with remote sensing*, pp. 533–575. Boca Raton, FL: CRC Press. January.
Soudani K, Hmimina G, Delpierre N, Pontailler JY, Aubinet M, Bonal D, Caquet B, de Grandcourt A, Burban B, Flechard C, et al. (2012) Ground-based network of NDVI measurements for tracking temporal dynamics of canopy structure and vegetation phenology in different biomes. *Remote Sensing of Environment* 123: 234–245.
Stow DA, Shih H-C, and Coulter LL (2014) Discrete classification approach to land cover and land use change identification based on Landsat image time sequences. *Remote Sensing Letters* 5(10): 922–931.
Tao F, Yokozawa M, Hayashi Y, and Lin E (2003) Changes in agricultural water demands and soil moisture in China over the last half-century and their effects on agricultural production. *Agricultural and Forest Meteorology* 118(3–4): 251–261.
Uchida E, Xu J, and Rozelle S (2005) Grain for green: cost-effectiveness and sustainability of China's conservation set-aside program. *Land Economics* 81(2): 247–264.
van der Werf GR, Morton DC, DeFries RS, Olivier JGJ, Kasibhatla PS, Jackson RB, Collatz GJ, and Randerson JT (2009) CO_2 emissions from forest loss. *Nature Geoscience* 2(11): 737–738.
Wang C and Maclaren V (2012) Evaluation of economic and social impacts of the sloping land conversion program: A case study in Dunhua county, China. *Forest Policy and Economics* 14(1): 50–57.
Woodcock CE, Allen R, Anderson M, Belward A, Bindchadler R, Cohen W, Gao F, Goward SN, Helder D, Helmer E, et al. (2008) Free access to landsat imagery. *Science* 320: 1011–1012.
Wu J (2006) Landscape ecology, cross-disciplinarity, and sustainability science. *Landscape Ecology* 21(1): 1–4.
Wulder MA (1998) Optical remote sensing techniques for the assessment of forest inventory and biophysical parameters. *Progress in Physical Geography* 1998(22): 449–476.
Wunder S (2008) Payments for environmental services and the poor: Concepts and preliminary evidence. *Environment and Development Economics* 13(03): 279–297.
Xie Y, Sha Z, and Yu M (2008) Remote sensing imagery in vegetation mapping: A review. *Journal of Plant Ecology* 1(1): 9–23.
Xu J, Bull GQ, Nilsson S, White A, and Pottinger A (2004) Forestry in China—Policy, consumption and production in forestry's newest superpower. *International Forestry Review* 6: 151.
Xu J, Tao R, Xu Z, and Bennett MT (2010) China's sloping land conversion program: Does expansion equal success? *Land Economics* 86(2): 219–244.
Yang X, Zhang J, and Wu T (2009) Social network structure and cooperation model of cross-border tourism region: A case study of Tiantangzhai in Dabieshan. *Acta Geographica Sinica* 64(8): 978–988.
Zhang Y and Song C (2006) Impacts of afforestation, deforestation, and reforestation on forest cover in China from 1949 to 2003. *Journal of Forestry* 104(7): 383–387.
Zong Y and Chen X (2000) The 1998 flood on the Yangtze, China. *Natural Hazards* 22(2): 165–184.